

## Short-range ordering in $\text{Al}_x\text{Ga}_{1-x}\text{As}$ grown with metal-organic vapor-phase epitaxy

A. J. Heinrich, M. Wenderoth,\* K. J. Engel, T. C. G. Reusch, K. Sauthoff,  
and R. G. Ulbrich

4. Physikalisches Institut der Universität Göttingen, Göttingen, Germany

E. R. Weber

Department of Materials Science, University of California at Berkeley, Berkeley, California 92775

K. Uchida

Tsukuba National Laboratories, Tsukuba, Japan

(Received 5 October 1998)

Atomically resolved, cross-sectional scanning tunneling microscopy was used to identify Al atoms in the surface layer of  $\text{Al}_{0.15}\text{Ga}_{0.85}\text{As}$  grown with metal-organic vapor-phase epitaxy. Characteristic fingerprints of individual and clusters of Al atoms were analyzed to identify surface-layer Al atoms resulting in atom maps of the Al positions. By quantitatively comparing the measured Al configuration with simulated images of a random Al incorporation, statistically significant deviations of the measured from a random Al distribution were found. These deviations are explained with a clear tendency of the Al atoms to form short-range ordered structures in the GaAs matrix. This ordering results in strings of Al atoms of a length of up to five Al atoms along low-indexed crystallographic directions. [S0163-1829(99)05415-6]

The  $\text{Al}_x\text{Ga}_{1-x}\text{As}$  ternary compound semiconductor is the most intensively investigated semiconductor alloy system used for the fabrication of heterostructures for industrial applications and fundamental research. The alloy structure of  $\text{Al}_x\text{Ga}_{1-x}\text{As}$  grown with molecular beam epitaxy (MBE) has been studied by several groups using transmission electron microscopy<sup>1</sup> (TEM) and also cross-sectional scanning tunneling microscopy (XSTM).<sup>2-4</sup>  $\text{Al}_x\text{Ga}_{1-x}\text{As}$  grown with metal-organic vapor-phase epitaxy (MOVPE) has been investigated by TEM.<sup>5,6</sup> The main advantage of XSTM, namely, the ability to determine local concentrations of the constituting components without averaging over many unit cells as in TEM, was recently applied to this system.<sup>7</sup>

Using XSTM on dilute  $\text{Al}_x\text{Ga}_{1-x}\text{As}$  with an average Al concentration of 2–3%, Smith *et al.* were able to identify and exactly localize first and second layer Al atoms.<sup>8</sup> By analyzing the distribution of the Al atoms determined in real space, they concluded that these are *distributed purely randomly* in the MBE-grown material with low Al concentration. In contrast to that, several authors remarked that Al atoms tend to cluster on typical length scales of a few unit cells at higher Al concentrations of  $x=30\%$  to  $40\%$ .<sup>4,9</sup> In addition, it was remarked that strings of Al atoms extend over several unit cells along the surface diagonals in some of these samples.<sup>2,4</sup> In addition, structural inhomogeneities influence the dynamic properties of alloys.<sup>10</sup> The existence of intrinsic microscopic clustering was, e.g., proposed as a model to explain the significant charge transfer over thick  $\text{Al}_x\text{Ga}_{1-x}\text{As}$  barriers.<sup>11</sup> A more quantitative approach to studying short-range order was used by Chao *et al.* in  $\text{In}_x\text{Ga}_{1-x}\text{As}$  alloys.<sup>12</sup> The authors analyzed their atom maps with a two-dimensional pair-correlation function and were able to derive the interaction energy of the In atoms.

In this paper we investigate the distribution of Al atoms in  $\text{Al}_{0.15}\text{Ga}_{0.85}\text{As}$  grown with MOVPE. We quantitatively com-

pare the measured Al pair-correlation functions with simulated images of random Al incorporation and show that Al atoms have a clear tendency to form short-range ordered structures.

All experiments were performed in an ultrahigh-vacuum chamber especially designed for XSTM work with a base pressure of better than  $5 \times 10^{-11}$  mbar. Polycrystalline tungsten tips were etched electrochemically, annealed, and sputter cleaned in the vacuum system. The samples were grown by MOVPE on (001) aligned GaAs substrates and for this study (110) surfaces were produced by *in situ* cleavage. The heterostructure consists of five pairs of (50 nm  $\text{Al}_{0.15}\text{Ga}_{0.85}\text{As}$ )/(50 nm GaAs) and was grown at a temperature of 620 °C with TMGa, TMAI, and  $\text{AsH}_3$  as precursors.  $\text{SiH}_4$  was added to obtain an *n*-type doping level of  $1 \times 10^{18} \text{ cm}^{-3}$ .

A large-scale, filled-state XSTM image of (50 nm)<sup>2</sup> of the  $\text{Al}_{0.15}\text{Ga}_{0.85}\text{As}/\text{GaAs}$  heterostructure is shown in Fig. 1. In the left half of the image an interface between GaAs and  $\text{Al}_{0.15}\text{Ga}_{0.85}\text{As}$  can be seen with some point defects such as vacancies and adsorbates in the GaAs. In the  $\text{Al}_{0.15}\text{Ga}_{0.85}\text{As}$  a large number of atomic-size electronic contrasts related to the Al atoms is seen; they are used in this paper to identify individual and pairs of surface-layer Al atoms on the atomic scale. Second layer Al atoms cannot be seen in these samples due to the relatively high concentration of Al atoms.<sup>8</sup>

The electronic contrasts related to the Al atoms can be seen in more detail in small-scale images with high-quality atomic resolution. Figure 2 shows a  $9 \text{ nm} \times 7 \text{ nm}$  image of one of the  $\text{Al}_{0.15}\text{Ga}_{0.85}\text{As}$  layers measured at a sample voltage of  $V_s = -2.5 \text{ V}$  and a tunnel current of  $I_T = 300 \text{ pA}$ .<sup>13</sup> According to the negative sample voltage, the filled As-related states are imaged.<sup>14</sup> In a first step, the atomic-size, electronic contrasts have to be linked to the positions of Al atoms. For this step, it is helpful to imagine the

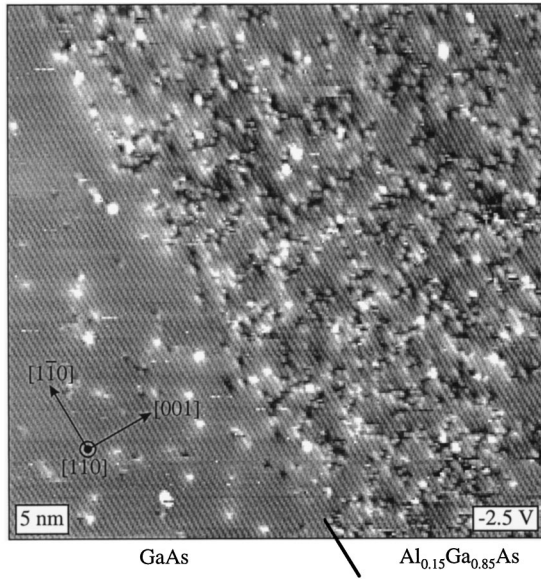


FIG. 1.  $(50 \text{ nm})^2$  filled-state XSTM image of the GaAs/ $\text{Al}_{0.15}\text{Ga}_{0.85}\text{As}$  heterostructure. The interface between GaAs (on the left) and  $\text{Al}_{0.15}\text{Ga}_{0.85}\text{As}$  (on the right) can be seen in the left half of the image; crystallographic directions are indicated.

$\text{Al}_{0.15}\text{Ga}_{0.85}\text{As}$  layers as a GaAs matrix with point defects introduced into the GaAs by individual Al or pairs of Al atoms. In such an approach the contrasts related to the Al atoms can be understood as “point defects” in the GaAs host material. At the Al concentration of  $x=15\%$  studied here, this is still feasible whereas at significantly higher Al concentrations ( $\geq 25\%$ ) this approach breaks down.

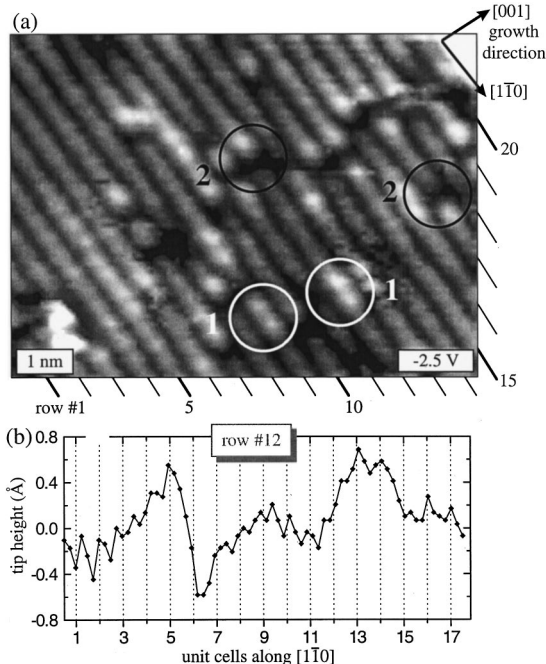


FIG. 2. (a) Al-rich area in the MOVPE-grown  $\text{Al}_{0.15}\text{Ga}_{0.85}\text{As}$  layer with Al-related electronic contrasts. Class 1 contrasts are marked with white circles and class 2 contrasts with black circles. Numbers mark the  $[1\bar{1}0]$  rows for discussion in the text. A cross section of row no. 12 is shown in (b).

In the following we classify the Al-related, electronic contrasts according to the morphology in the filled-state XSTM images: A first class of Al-related point defects in the GaAs matrix is induced by an individual surface Al atom on a Ga site as discussed by Smith *et al.*<sup>8</sup> Two examples are marked with white circles in Fig. 2(a) showing two enhanced As atoms along the  $[1\bar{1}0]$  zigzag chains.

Two examples of a second class of “point defects” are marked with black circles in Fig. 2(a). These consist of neighboring enhanced and depressed As atoms along the  $[1\bar{1}0]$  direction. This can be seen clearly in the cross section of row no. 12 shown in Fig. 2(b). In that cross section a class 2 “point defect” with its dipolelike contrast and a class 1 “point defect” intersect. For the class 2 features the depressed As atom appears  $0.5 \text{ \AA}$  lower and the enhanced As atom  $0.4 \text{ \AA}$  higher than the average height. In contrast to the dipolelike center of the class 2 “defect,” which appears atomically abrupt, the sides of this defect stretch over several unit cells along the  $[1\bar{1}0]$  direction. Note that the class 2 contrasts exist in two variants which have opposite symmetry along the zigzag chains.

It is important to notice that an asymmetric electronic contrast along a zigzag chain in a filled-state image cannot be caused by a single point defect on the group III sublattice due to the inherent symmetry of the  $\{110\}$  surfaces. We therefore conclude that the second class of “point defects” is due to a paired defect of an Al atom on a Ga site with another point defect. Three plausible partners of the surface Al atom can be used to explain the symmetry and occurrence of two variants of the class 2 features: (i) an As vacancy adjacent to the surface Al atom, (ii) a H adsorbate at an As atom adjacent to the Al atom, or (iii) an additional subsurface Al atom in the backbond of one As atom.<sup>15,16</sup>

In the case where the asymmetric contrasts are caused by a subsurface Al atom in addition to the surface-layer Al atom, the two As neighbors of the surface Al atom in the zigzag chain are distinguished by the fact that only one of them has a second Al atom in its back-bond. Under the simple assumption of random Al occupation of the first subsurface layer this configuration would be obtained for 40% of the Al-related contrasts. On the other hand, the density of surface vacancies and adsorbates should increase notably with time of the order of several hours. Hence the density of class 2 features should increase while the density of class 1 features should decrease with time. This effect has not been observed by us and has also not been reported by other groups.

It is important to note that all three models for the class 2 “defect” given here have an Al atom on a surface Ga site in common. Therefore these contrasts can be used to localize surface-layer Al atoms, independent of the exact “chemical” nature of the partner.

Examples for extended Al-related contrasts are also abundant in our samples. Figure 3 shows strings of Al atoms along the  $[1\bar{1}2]$  direction on the left and along  $[1\bar{1}\bar{2}]$  on the right which are extended over several unit cells. Later we will show that these strings are clear examples for the tendency of Al atoms to form short-range ordered structures in MOVPE-grown  $\text{Al}_x\text{Ga}_{1-x}\text{As}$ . A plausible explanation for the dipolelike contrasts of these strings is again the incorpo-

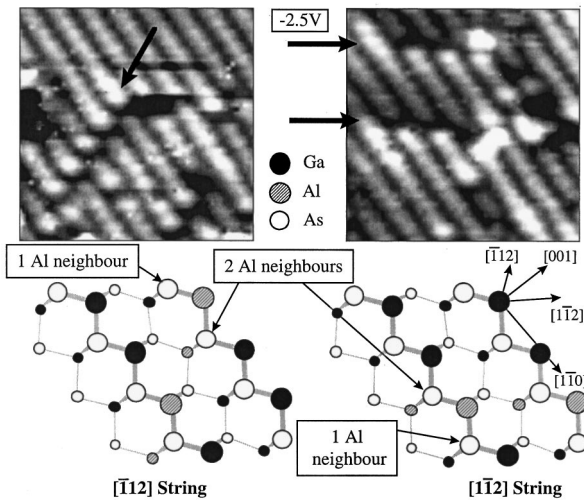


FIG. 3. Strings of Al atoms along  $[1\bar{1}2]$  and  $[\bar{1}12]$  extending over several unit cells. The ball and stick models include surface (large symbols) and first subsurface (small) atoms.

ration of subsurface Al atoms underneath the string of Al atoms in the surface layer. This model configuration is shown in the ball and stick models underneath each XSTM image. In the case of these strings, the interpretation of the dipolelike contrasts as H adsorbates or As vacancies appears less likely than the subsurface Al atoms. On the one hand, all strings show exactly the same symmetry of the electronic contrast as shown in Fig. 3, which can easily be understood in the model of subsurface Al atoms due to the fixed atomic structure of the crystal [either a  $(110)$  or a  $(1\bar{1}0)$  surface]. On the other hand, an adsorbate or an As vacancy could be to the right or the left of the string of surface Al atoms and we would therefore expect a change of the dipolelike contrasts along a string.

In the model of a subsurface string of Al atoms there are some surface As atoms with one and others with two Al neighbors. If the string is oriented along the  $[\bar{1}12]$  direction (left image of Fig. 3), surface As atoms to the left of the string have only one Al neighbor and these are imaged as the enhanced As atoms (white contrast). On the other hand, the surface As atoms with two Al neighbors on the right of the string are imaged as depressed As atoms (black contrast). This observation holds equally for the Al string along the  $[1\bar{1}2]$  direction (right image). Again those surface As atoms with one Al neighbor are imaged as enhanced and those with two Al neighbors as depressed atoms.

With these identifications of the exact positions of surface-layer Al atoms in mind, spatial pair-distribution functions of the Al atoms can be calculated from atom maps derived from the measured XSTM images. A similar approach was used by Smith *et al.* on dilute MBE-grown  $\text{Al}_x\text{Ga}_{1-x}\text{As}$  with  $x=0.03$  where the authors found no significant deviations of the measured from the random Al distribution.<sup>8</sup>

Figure 4 shows a XSTM image used for a quantitative analysis of the Al pair-distribution function of the  $\text{Al}_{0.15}\text{Ga}_{0.85}\text{As}$  layers. The imaged surface area is  $(19\text{ nm})^2$  and the total number of group III surface sites in the image is 1597, leading to an expected number  $N$  of 240 Al atoms.

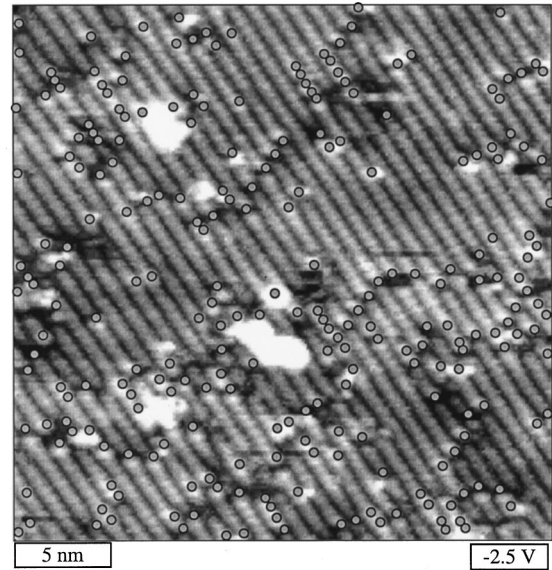


FIG. 4.  $(19\text{ nm})^2$  surface area of the  $(110)$  surface of  $\text{Al}_{0.15}\text{Ga}_{0.85}\text{As}$  used for a quantitative analysis of the distribution of the Al atoms. The atom map of the positions of the surface Al atoms is superimposed on the image. Some adsorbates extend over several atomic sites.

Three areas of this surface are covered by adsorbates from the residual gas of the vacuum system which adsorb preferentially on the  $\text{Al}_{0.15}\text{Ga}_{0.85}\text{As}$ .<sup>9</sup> At these locations, the original surface configuration cannot be seen. The positions of the Al atoms as determined from the XSTM image can be seen superimposed on the image. 254 Al atoms were clearly identifiable via the characteristic contrasts of class 1 and class 2 features as described above. This is in reasonable agreement with the expected number of  $N=240$  Al atoms (statistical error due to the finite size of the image:  $\pm 15$  Al atoms).

In a qualitative view, the Al atoms in the XSTM image of Fig. 4 are not located randomly on the group III sublattice. Rather there seem to be short-range correlations in the form of strings of Al atoms (as shown in Fig. 3) and long-range modulations of the local Al concentration. These qualitative descriptions of the nonrandom distribution of Al atoms in the  $\text{Al}_{0.15}\text{Ga}_{0.85}\text{As}$  can be quantified by comparing the measured atom maps with simulated maps of a purely random Al incorporation. Such an approach was described recently by Smith *et al.* for MBE-grown  $\text{Al}_{0.15}\text{Ga}_{0.95}\text{As}$  where the authors concluded that the Al atoms are incorporated randomly on the group III sublattice in that material.<sup>8</sup>

Figure 5(a) shows the number  $N_r$  of Al atoms in a shell of width  $5\text{ \AA}$  plotted as a function of the distance  $r$  from a central Al atom for the measured atom map of Fig. 4. The same procedure is done for 1000 simulated atom maps of exactly the same size as the XSTM image but with a random Al distribution, those values  $N_{\text{rand}}$  are shown in Fig. 5. For this evaluation the numbers for an individual central Al atom were added over all Al atoms, which gives the total numbers  $N_r$  and  $N_{\text{rand}}$ . Both total numbers rise linearly with distance up to about  $100\text{ \AA}$  because they are proportional to the area of the shell at distance  $r$ . In this linear part, a fine structure is visible in both curves which is due to the discrete atomic

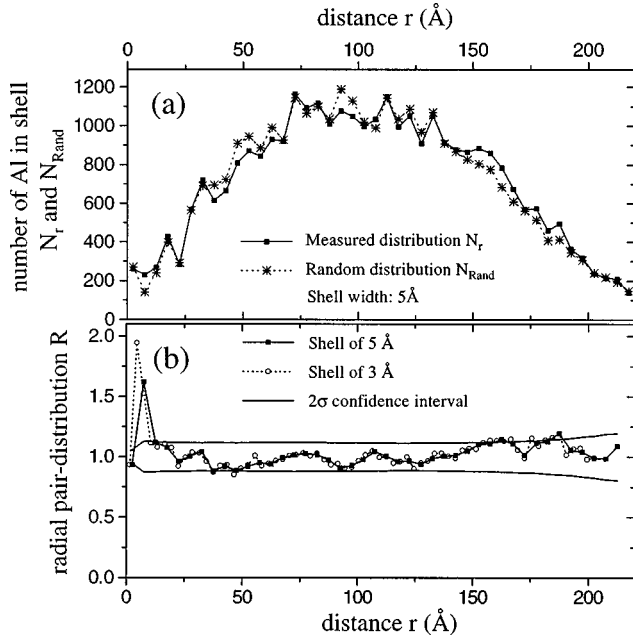


FIG. 5. (a) Number of Al atoms in the measured and in the simulated random atom maps in a shell of width 5 Å as a function of the distance  $r$  from a central Al atom. (b) The radial pair-distribution function  $R$  of the measured atom map.

positions in the lattice. At distances larger than about 100 Å the total numbers decrease because of the finite size of the atom map of  $(19 \text{ nm})^2$ .

Due to the complex structure of the curves it is evident that a comparison of the measured to simulated distributions is needed. Such a comparison can be done by normalizing the measured with the simulated, random distribution which gives the radial pair-distribution function  $R(r)$ :

$$R(r) = N_r(r) / N_{\text{rand}}(r).$$

The radial pair-distribution function for the measured atom map of Fig. 4 is shown in Fig. 5(b). Due to the normalization, a radial pair-distribution value of 1 is in agreement with the hypotheses that the Al atoms are distributed purely randomly on the cation sublattice. A comparison of two shells of widths 3 and 5 Å is included in Fig. 5(b) with significant differences only at small distances  $r$ . In order to determine the statistical significance of features in the pair-distribution function, the standard deviation  $\sigma$  was determined from the simulated random Al distributions and is included in Fig. 5(b) as the  $2\sigma$  confidence interval around the mean of the statistical distribution. The expected error in  $N_{\text{rand}}$  can be estimated as follows:

$$N_{\text{rand}}(r) = \sum_{i=1}^N N_{r,\text{individual}}^i \approx N \times N_{r,\text{individual}},$$

with  $N_{r,\text{individual}}^i$  the number of Al atoms in the shell around the  $i$ th Al atom. The statistical error in  $N_{\text{rand}}$  depends (i) on the error in the total number of Al atoms  $N$  in each simulated atom map and (ii) on the error in  $N_{r,\text{individual}}$  which is proportional to the square root of the distance. In the normalized representation of  $R(r)$  the total error is dominated by the distribution of the total number of Al atoms and is indepen-

dent of  $r$  as shown in Fig. 5(b). On the other hand, the increase at large  $r$  is due to the smaller total numbers in each individual shell  $N_{r,\text{individual}}$  (due to the finite size of the measured and simulated images).

The radial pair-distribution function in Fig. 5(b) shows two types of deviations of the measured from the random distribution. First, there is a pronounced enhancement of short distances of about 3–10 Å in the measured distribution. These are about 1.5 to 2 times more abundant than in the random model, depending on the shell width, and lie at about  $5\sigma$  from the expectation value for the random Al distribution. Hence with a statistical significance of about 99%, the assumption that the Al atoms are distributed randomly on the cation sublattice has to be rejected. This increase of short-distance pairs indicates a tendency of the Al atoms to form short-range ordering. Secondly, the radial pair-distribution function shows a modulation at larger distances with an approximate period of 40–50 Å. This modulation corresponds to the qualitative description of Al-rich and Al-poor areas on a long length scale which can be clearly seen in Fig. 1. But the standard deviation shows that the radial pair-distribution function is not the correct analysis to prove that these long-range modulations are indeed statistically significant. In this case a cluster analysis would be needed.

In the following, we focus on the anisotropic correlations of the Al atoms, which are not included in the radial pair correlation but are expected for short-range ordering. The XSTM image of Fig. 3 showed strings of Al atoms extending up to five atoms. To show quantitatively that this is a clear deviation from a random distribution of the Al atoms, Fig. 6 compares the numbers  $A(\mathbf{k}, l)$  of such strings with given length  $l$  and direction  $\mathbf{k}$  as determined from the measured atom map with those expected for a random distribution  $A_{\text{rand}}(\mathbf{k}, l)$ . Longer Al strings are also counted as shorter strings in both distributions, i.e., a string of length 4 appears twice as length 3 and three times as length 2. As a consequence the total number of strings of length 2 gives the number of Al pairs along the given direction, the value of the pair distribution along this direction.

Again it is very important to compare the results from the measured Al atom maps with those from the assumption that the Al atoms are distributed randomly. In a one-dimensional model (along the direction  $\mathbf{k}$ ), the expectation value  $A_{\text{rand}}$  for the number of strings of Al atoms of a given length can be easily calculated from elementary combinatorial steps to be

$$A_{\text{rand}}(N, l) = (N - l + 1)x^l,$$

with  $l$  the length of the Al string,  $N$  the total number of sites, and  $x$  the probability of occupying a site with Al. From this one-dimensional result it is straightforward to add the expectation values  $A_{\text{rand}}(N, l)$  for all lines along a given crystallographic direction to obtain the total number of strings  $A_{\text{rand}}(l)$  of length  $l$  in a measured or simulated two-dimensional atom map. The standard deviation from this expectation value does not have a closed analytical form such as the expectation value and is hence best determined from a large number of simulated atom maps with random Al distribution.

Two low-indexed directions are evaluated in Fig. 6, namely, the two surface unit cell diagonals  $[1\bar{1}2]$  and  $[\bar{1}12]$ .<sup>3,5,17</sup> It

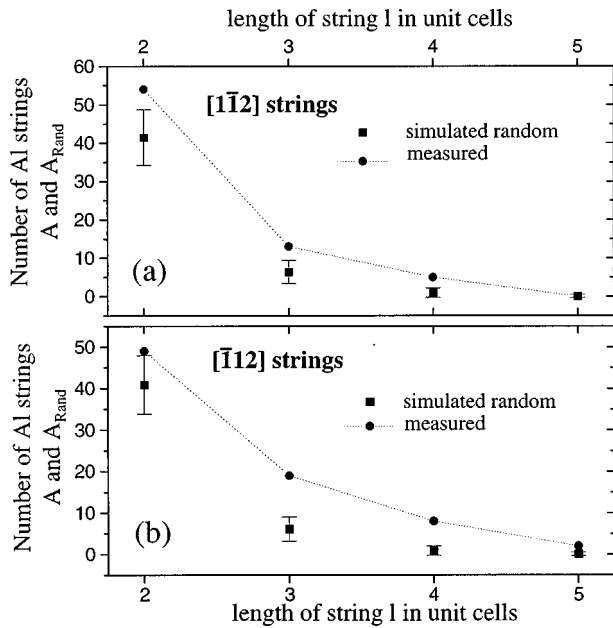


FIG. 6. Number of strings of Al atoms along  $[1\bar{1}\bar{2}]$  and  $[\bar{1}\bar{1}\bar{2}]$  as a function of the length of the string  $k$  for the measured and the random atom maps.

can be seen in both directions that the measured numbers of Al pairs (strings of length  $l=2$ ) along these directions are a little higher than in a random Al distribution but that this is just outside the  $1\sigma$  standard deviation and hence statistically not too significant. In contrast to that, strings of length 3 lie about  $4\sigma$  ( $2\sigma$ ), strings of length 4 about  $6\sigma$  ( $3\sigma$ ) from the expectation value  $A_{\text{rand}}$  for the  $[\bar{1}\bar{1}\bar{2}]$  direction ( $[1\bar{1}\bar{2}]$ , respectively). From this we can quantitatively prove that the strings of Al atoms along the  $[1\bar{1}\bar{2}]$  and the  $[\bar{1}\bar{1}\bar{2}]$  directions cannot be explained with the assumption of a statistical distribution of the Al atoms on the cation sublattice with a statistical significance of more than 99%. Hence we obtain the result that the Al atoms have a strong tendency to form strings along some low-indexed directions in MOVPE-grown  $\text{Al}_{0.15}\text{Ga}_{0.85}\text{As}$ .

The strings of Al atoms observed here are a form of short-range ordering, in this case resulting in an increased prob-

ability of having like atoms along the  $[1\bar{1}\bar{2}]$  and  $[\bar{1}\bar{1}\bar{2}]$  directions.<sup>18</sup> Those strings are most likely formed during the MOVPE growth process. Here the question arises whether these strings at the surface are truly one dimensional or rather two dimensional, extending beneath the (110) surface studied here.<sup>19</sup> From the model interpretation of the electronic contrast of the Al strings given above including first and second layer Al strings we conclude that these strings are indeed part of AlAs platelets. In that case the AlAs platelets would be extended on Al-rich  $\{111\}_B$  planes. These platelets could be compared with the separation of the two isoivalent components on the cation sublattice in long-range ordered ternary compound semiconductors.<sup>18</sup> Whereas the reported long-range ordered structure for  $\text{Al}_x\text{Ga}_{1-x}\text{As}$  alloys is  $\text{CuAu}$ , it is well known that long-range  $\text{CuPt}_B$  ordering with ordering on  $\{111\}_B$  planes is energetically favorable for many materials.<sup>20–22</sup> In this context the AlAs platelets discussed here would be the initial state of  $\text{CuPt}_B$  ordered  $\text{Al}_x\text{Ga}_{1-x}\text{As}$ .

In summary, using cross-sectional scanning tunneling microscopy we were able to show that Al atoms in  $\text{Al}_{0.15}\text{Ga}_{0.85}\text{As}$  grown with metal-organic vapor-phase epitaxy have a strong tendency to form short-range ordered structures in the GaAs matrix. To facilitate such a quantitative analysis, the exact positions of the Al atoms in the (110) cleavage surface had to be determined. From the symmetries of the Al-related electronic contrasts we identified individual Al atoms in the surface as well as pairs of Al atoms with a point defect. Using these characteristic fingerprints of the Al atoms, we were able to derive atom maps of the Al positions from XSTM images.

The measured atom maps were compared to simulated atom maps with a purely random Al incorporation. The radial pair-distribution function indicated that there is a statistically significant enhancement of short-distance Al neighbors. In addition, long-range modulations were seen which can be explained by modulations in the local Al concentration with a length scale of about 5 nm. The short-distance features were then shown to be largely due to strings of Al atoms extended along the  $[1\bar{1}\bar{2}]$  and the  $[\bar{1}\bar{1}\bar{2}]$  directions which can with a high probability not be explained with the basic assumption that the Al atoms are distributed randomly on the cation sublattice.

\*Author to whom correspondence should be addressed. Electronic address: wendero@physik4.gwdg.de

<sup>1</sup>A. Ourmazd, D. W. Taylor, J. Cunningham, and C. W. Tu, *Phys. Rev. Lett.* **62**, 933 (1989).

<sup>2</sup>M. B. Johnson, U. Maier, H. P. Meier, and H. W. M. Salemink, *Appl. Phys. Lett.* **63**, 1273 (1993).

<sup>3</sup>S. Gwo, K. J. Chao, C. K. Shih, K. Sadra, and B. G. Streetman, *Phys. Rev. Lett.* **71**, 1883 (1993).

<sup>4</sup>A. R. Smith, K. J. Chao, C. K. Shih, Y. C. Shih, and B. G. Streetman, *Appl. Phys. Lett.* **66**, 478 (1995).

<sup>5</sup>J. Kim, J. J. Alwan, D. V. Forbes, J. J. Coleman, I. M. Robertson, C. M. Wayman, F. H. Baumann, M. Bode, Y. Kim, and A. Ourmazd, *Appl. Phys. Lett.* **61**, 28 (1992).

<sup>6</sup>G. B. Stringfellow and G. S. Chen, *J. Vac. Sci. Technol. B* **9**, 2182 (1991).

<sup>7</sup>A. J. Heinrich, M. Wenderoth, M. A. Rosentreter, K. Engel, M. A. Schneider, R. G. Ulbrich, E. R. Weber, and K. Uchida, *Appl.*

*Phys. A: Mater. Sci. Process.* **66**, 959 (1998).

<sup>8</sup>A. R. Smith, K. J. Chao, C. K. Shih, K. A. Anselm, A. Srinivasan, and B. G. Streetman, *Appl. Phys. Lett.* **69**, 1214 (1996).

<sup>9</sup>H. W. M. Salemink and O. Albrechtsen, *Phys. Rev. B* **47**, 16 044 (1993).

<sup>10</sup>L. El. Mir and J. C. Bourgoin, *Phys. Status Solidi B* **207**, 577 (1998).

<sup>11</sup>D. S. Kim, H. S. Ko, Y. M. Kim, S. J. Rhee, S. C. Hohng, Y. H. Yee, W. S. Kim, J. C. Woo, H. J. Choi, J. Ihm, D. H. Woo, and K. N. Kang, *Phys. Rev. B* **54**, 14 580 (1996).

<sup>12</sup>K. J. Chao, C. K. Shih, D. W. Gotthold, and B. G. Streetman, *Phys. Rev. Lett.* **79**, 4822 (1997).

<sup>13</sup>It should be noted that the vast majority of XSTM images of  $\text{Al}_x\text{Ga}_{1-x}\text{As}$  are filled-state images; an exception can be found in Ref. 9.

<sup>14</sup>R. M. Feenstra, J. A. Stroscio, J. Tersoff, and A. P. Fein, *Phys. Rev. Lett.* **58**, 1192 (1987).

- <sup>15</sup>S. B. Zhang and A. Zunger, Phys. Rev. Lett. **77**, 119 (1996).
- <sup>16</sup>Ph. Ebert, X. Chen, M. Heinrich, M. Simon, K. Urban, and M. G. Lagally, Phys. Rev. Lett. **76**, 2089 (1996).
- <sup>17</sup>The determination of strings of Al atoms along the  $[1\bar{1}0]$  direction (along the zigzag chains) is not unambiguous from filled-state XSTM images and is therefore omitted here. This is primarily due to the fact that a single surface Al atom extends over two As sites in a filled-state image. This difficulty does not exist along the two directions analyzed here.
- <sup>18</sup>A. Zunger and S. Mahajan, in *Handbook on Semiconductors*, edited by T. S. Moss (Elsevier, Amsterdam, 1994), pp. 1399–1514.
- <sup>19</sup>A XSTM study of the (110) and the  $(1\bar{1}0)$  of samples taken from the same MOVPE-grown wafer is planned for the future.
- <sup>20</sup>T. S. Kuan, T. F. Kuech, W. I. Wang, and E. L. Wilkie, Phys. Rev. Lett. **54**, 201 (1985).
- <sup>21</sup>A. Gomyo, T. Suzuki, and S. Iijima, Phys. Rev. Lett. **60**, 2645 (1988).
- <sup>22</sup>S. B. Zhang, S. Froyen, and A. Zunger, Appl. Phys. Lett. **67**, 3141 (1995).